Negative-Differential-Resistance Devices Achieved by Band-Structure Engineering in Silicene under Periodic Potentials

Chang-Hung Chen,[1,2,*,†] Wen-Wu Li,[1,*] Yuan-Ming Chang,[2] Che-Yi Lin,[3] Shih-Hsien Yang,[4] Yong Xu,[5,‡] and Yen-Fu Lin[2,§]

[1]*Key Laboratory of Polar Materials and Devices (Ministry of Education), Technical Center for Multifunctional Magneto-Optical Spectroscopy (Shanghai), East China Normal University, Shanghai 200241, China*
[2]*Department of Physics, National Chung Hsing University, Taichung 40227, Taiwan*
[3]*Department of Electrophysics, National Chiao Tung University, Hsinchu 30010, Taiwan*
[4]*Institute of Electronics Engineering, National Tsing Hua University, Hsinchu 30013, Taiwan*
[5]*School of Electronic and Optical Engineering, Nanjing University of Posts and Telecommunications, Nanjing, Jiangsu, 210023, China*

An important development in modern electronics is the realization of band-structure engineering for the design of novel materials and devices. One possible way to realize band-structure engineering is by addition of periodic potentials to two-dimensional (2D) materials, such as graphene, to form a superstructure, known as a "superlattice.' Unlike the band gap of graphene, the band gap of silicene can be tuned by an out-of-plane electric field owing to its unusual buckled structure. In this work, we use the designable band gap of silicene and the band structure of superlattices, together with the spin and valley degrees of freedom, to propose a design principle for optimizing the performance of spin- and valley-dependent negative-differential-resistance (NDR) devices using silicene superlattices. On the basis of the effective Hamiltonian formalism, we predict that the peak-to-valley current ratio could be larger than most recently reported results achieved by 2D materials, suggesting that the silicene superlattice is a good candidate for realizing NDR devices. The design principle proposed in this work could also be extended to other layered materials with tunable band gaps. This could pave the way for advanced material and device designs based on band-gap engineering of 2D materials.

I. INTRODUCTION

Since the experimental realization of graphene [1], two-dimensional (2D) materials have been intensely investigated in condensed-matter physics. It has been shown that the band gap of some 2D materials, such as bilayer graphene [2] and trilayer graphene [3], can be tuned by an electric field. Silicene is a 2D artificial honeycomb-like lattice made of Si atoms. In contrast to monolayer graphene, for which the A and B sublattices are in the same plane, the buckled structure of silicene allows easy control of its band diagram as well as its band gap by the application of an out-of-plane electric field [4]. Furthermore, silicene possesses two other advantages. First, owing to its honeycomb lattice, silicene shares many of the prominent properties of graphene, such as a high Fermi velocity and carrier mobility, which are superior to those of traditional semiconductor materials. Second, silicene has greater compatibility with current silicon-based technologies compared with graphene and other 2D materials. The superior properties of silicene make it an attractive material for the development of next-generation electronics [5].

In addition to the tunability of the band gap in 2D materials with the use of an out-of-plane electric field, band-gap engineering can also be realized by addition of periodic potentials to form a superstructure, or superlattice, of an artificial crystal [6]. The band structure of a superlattice can be tailored by adjustment of the parameters of the superlattice, such as the lattice constant. The band-structure engineering achieved by the superlattice structure is helpful for optimizing the performance of devices. Although the concept of superlattices was proposed many years ago, the physics community has recently showed intense interest in graphene superlattices, owing to their intriguing properties, such as anisotropic behaviors of massless Dirac fermions, superlattice Dirac points, topological current, and ballistic miniband conduction [7–13]. The advantages of silicene mentioned above

---

*C.-H. Chen and W.-W. Li contributed equally to this work.
†chchen0428@gmail.com
‡xuyong.hn@gmail.com
§yenfulin@nchu.edu.tw

suggest it would be interesting to study band-gap engineering of silicene in addition to its superlattice properties. However, relatively few papers have been published on this topic to date [14–18].

Negative-differential-resistance (NDR) devices have gained much attention owing to their peculiar folded current-voltage characteristics (N-shaped I_{SD}-V_{SD} curves), which present multiple threshold-voltage values. These features are of interest for the design of new functionalities, such as reflection amplifiers, memories, and oscillators [19–21]. Very recently, NDR devices based on 2D layered materials have been explored [22–29]. Multivalued logic circuits have been implemented with NDR electronics based on complex 2D layered heterojunction channels, in which the power consumption is lower than that of conventional binary systems as expected from theoretical predictions [29]. Additionally, a high peak-to-valley current ratio (PVCR) of 4.2 has been achieved at room temperature. Through the construction of superlattices on 2D conducting channels for local band-structure engineering, NDR electronics can be achieved and a higher PVCR might also be possible in future circuit design. To the best

of our knowledge, there have been no investigations of the NDR effect in silicene superlattices.

In the present work, we use band-gap engineering of both silicene and its superlattice to develop a design principle for optimizing the performance of spin- and valley-dependent negative-differential-resistance devices based on silicene superlattices. The structure of the proposed silicene superlattices is much simpler than that of complex layered 2D heterostructures. We show that the band gap of silicene, its lateral thicknesses, and the period of the superlattices have distinct effects on the band structure of the silicene superlattice. This band-structure design principle might be extended to other 2D materials with tunable band gaps, paving the way for advanced material and device design.

II. METHODS

A. Effective Hamiltonian formalism

The tight-binding Hamiltonian for silicene can be expressed as the sum of the simplest tight-binding model for graphene [37], spin-orbit interaction terms, and
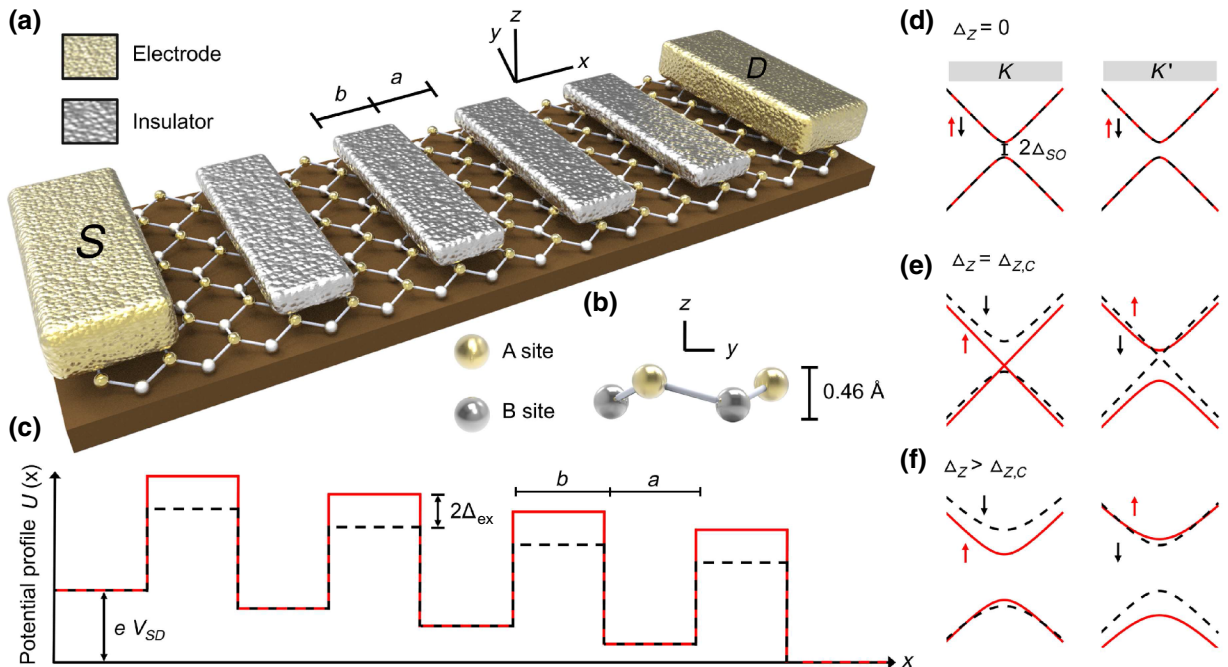

FIG. 1. Silicene superlattice structure, potential profile, and band structure. (a) The structure of a silicene superlattice, a silicene monolayer connected to source (S) and drain (D) electrodes, with four strips of ferromagnetic insulators on top. (b) Side view of silicene showing that the two sublattice atomic planes have a vertical separation distance of 0.46 Å, forming a buckled structure. (c) The potential profiles $U(x)$ for spin-up electrons (solid red line) and spin-down electrons (dashed black line). Δ_{ex} is the exchange-splitting energy induced by the ferromagnetic insulator. Schematic band structure of silicene around K and K' points for three different staggered sublattice potentials, (d) $\Delta_Z = 0$, (e) $\Delta_Z = \Delta_{Z,C}$, and (f) $\Delta_Z > \Delta_{Z,C}$, which can be induced by application of an out-of-plane electric field. $\Delta_{Z,C} = \Delta_{SO} = 3.9$ meV denotes the critical staggered sublattice potential where silicene becomes semimetallic for $K \uparrow$ and $K' \downarrow$.

staggered sublattice potential induced by external electric field E_Z:

$$H = -t \sum_{\langle i,j \rangle s} c_{is}^{\dagger} c_{js} + i \frac{\Delta_{SO}}{3\sqrt{3}} \sum_{\langle\langle i,j \rangle\rangle s} s v_{ij} c_{is}^{\dagger} c_{js}$$
$$- d \sum_{is} \mu_i E_Z c_{is}^{\dagger} c_{js}, \tag{1}$$

where t is the transfer energy, $c_{is}^{\dagger}$ is the creation operator for electrons with spin polarization $s = \uparrow\downarrow$ at site i, and $\langle i,j \rangle$ and $\langle\langle i,j \rangle\rangle$ run over the nearest-neighbor and the next-nearest-neighbor hopping sites, respectively. The parameter Δ_{SO} is the intrinsic SOI, $v_{ij} = +1$ (-1) for counterclockwise (clockwise) next-nearest-neighbor hopping, $\mu_i = +1$ (-1) for the A (B) site, and d is the buckled height of silicene. The low-energy physics that we are interested in can be described by the massive Dirac Hamiltonian:

$$H_0 = \hbar v_F (\tau k_x \sigma_x + k_y \sigma_y) + \Delta_{s\tau} \sigma_z, \tag{2}$$

where $v_F \approx 5.5 \times 10^5$ ms^{-1} is the Fermi velocity, $\widehat{\sigma}$ is the Pauli matrix, and $\Delta_{s\tau} = s\tau \Delta_{SO} - \Delta_Z$ is the band gap induced by SOI and the staggered sublattice potential. Notably, the massive Dirac Hamiltonian can also be used for other 2D materials, including germanene, stanene, and group-VIB transition-metal dichalcogenides [38]. In the presence of the exchange-splitting energy Δ_{ex} and gate voltage V_g, the Hamiltonian becomes

$$H = H_0 + (eV_g + \Delta_{ex}). \tag{3}$$

Similarly to graphene [35], the band structure and the transmission spectrum of silicene superlattices can be obtained on the basis of the effective Hamiltonian formalism.

III. RESULTS

A. Silicene superlattices

Figure 1(a) shows a schematic illustration of the proposed NDR device, a silicene superlattice composed of monolayer silicene on a substrate with $N = 4$ insulating strips on top of the silicene. Both ferromagnetic and nonmagnetic insulating strips are considered in this work. The results for the latter are provided in Supplemental Material [30]. Ferromagnetic insulators can induce an exchange-splitting energy Δ_{ex} in silicene via the proximity effect, as proposed and achieved for graphene [31–33]. Hallal *et al.* [33] found that the exchange splitting obtained in graphene ranges from tens to hundreds of millielectronvolts depending on the substrate. On the basis of the data from graphene, two groups individually used $\Delta_{ex} = 36$ meV [17] and $\Delta_{ex} = 100$ meV [34] in

their calculations as the exchange-splitting energy induced in silicene. In this work, we use $\Delta_{ex} = 36$ meV, a relatively conservative value, in our calculations. Higher Δ_{ex} is expected to achieve a spin- and valley-dependent NDR device with better performance. However, this energy will vanish with the use of nonmagnetic insulating strips. A top gate voltage is applied to the ferromagnetic or non-magnetic insulator to induce a barrier potential in the silicene. A bias voltage (V_{SD}) is applied through the source (S) and drain (D) electrodes. A schematic diagram of the potential profile used in the calculation is shown in Fig. 1(c).

B. Tunable band gap of silicene

The two sublattice atomic planes of silicene feature a vertical separation distance of $d = 0.46$ Å, forming a buckled structure, as shown in Fig. 1(b). By application of an out-of-plane electric field E_Z, this unique structure allows us to induce a staggered sublattice potential $\Delta_Z = E_z d$ [4]. Therefore, the band gap of silicene, $\Delta_{\tau s} = |\tau s \Delta_{SO} - \Delta_Z|$, can be controlled by the out-of-plane electric field. Here $\tau = +1$ (-1) and $s = +1$ (-1) denote the K (K') valley and spin-up (spin-down) degrees of freedom, respectively. $\Delta_{SO} = 3.9$ meV denotes the intrinsic spin-orbit interaction (SOI) of silicene. Figures 1(d) and 1(f) show the schematic band structure of silicene around K (left panel) and K' (right panel) points for three different staggered sublattice potentials, $\Delta_Z = 0$, $\Delta_Z = \Delta_{Z,C}$, and $\Delta_Z > \Delta_{Z,C}$, respectively, where $\Delta_Z = \Delta_{SO}$ is the critical staggered sublattice potential; that is, the critical point for the topological phase transition of silicene [4]. Notably, a topological phase transition can be achieved simply by the tuning of the staggered sublattice potential with the out-of-plane electric field in silicene. For $\Delta_Z = 0$ in the nonmagnetic region, the band gap of silicene is $2|\Delta_{SO}|$ for both the K valley and the K' valley [Fig. 1(d)]. In the magnetic region, for $\Delta_Z > \Delta_{Z,C}$, the band gap of silicene is $2|\tau s \Delta_{SO} - \Delta_{SO}|$ such that silicene is semimetallic for spin-up electrons in the K valley and for spin-down electrons in the K' valley [Fig. 1(e)]. For $\Delta_Z > \Delta_{Z,C}$, the band gap for spin-up electrons in the K valley and spin-down electrons in K' valley will open again [Fig. 1(f)]. As will be shown, the magnitude of the staggered sublattice potential is important for the performance of the proposed NDR device. The tunability of the staggered sublattice potential, and thus the band gap of silicene, makes it possible to optimize the device performance simply by adjustment of the magnitude of the electric field.

C. Band structure and transmission spectra

To understand the spin- and valley-dependent transport properties of the silicene superlattice, its band structure and transmission spectra are investigated on the basis of the effective Hamiltonian formalism similar to that for

graphene (see Sec. II) [7,35]. Figures 2(a) and 2(b) show the energy as a function of the y-component wave vector k_y and the Bloch-wave vector K_{sl}, respectively, for four combinations of spin and valley flavor, $K\uparrow$, $K\downarrow$, $K'\uparrow$, and $K'\downarrow$. The allowed and forbidden bands are formed, which are useful in understanding the electronic transport phenomena. In this work, the forbidden band formation is of crucial importance to obtain the NDR effect. The band gaps at $k_y = 0$ nm^{-1} in Fig. 2(a) correspond to those in Fig. 2(b). The band structures for each spin and valley combination are different, leading to spin and valley polarization, which is the origin of the spin- and valley-dependent NDR effect, as shown later. Fig. 2(c) shows the transmission spectra for a silicene superlattice with $N = 8$ barriers for $V_{SD} = 0$ V, with clear low-transmission regions corresponding to the band gaps in Figs. 2(a) and 2(b). Marks A and B denote two high-transmission regions, each containing $N - 1$ resonant peaks, corresponding to two allowed bands in the band structure. Fig. 2(d) shows the transmission spectrum as a function of bias voltage V_{SD} for spin-up electrons in the K' valley. For $V_{SD} = 0$ mV, this spectrum corresponds to the third panel in Fig. 2(c). For a small V_{SD}, the minibands evolve into Wannier-Starker ladders with suppression of the transmission spectrum, which is an important signature of a Bloch electron moving in a periodic structure under a bias voltage.

D. Bias-dependent transmission spectra

Next we investigate the bias-dependent transmission spectra by changing the designable parameters of the superlattices, including the period and lateral width, and the tunable staggered sublattice potential of the silicene. These parameters are shown to be useful for interpreting the current-voltage characteristics, and hence the NDR effect.

The effect of the number of barriers on the transmission spectra can be further understood from comparison of Fig. 3(a) (eight barriers) and Fig. 3(b) (four barriers). In Fig. 3(b), the four thick black lines (denoted by numbers 1 to 4) with a transmission of almost zero originate from the band gap of the silicene in the four barrier regions with a magnitude of $2(\Delta_{SO} + \Delta_Z)$. Similarly, the three thin lines (denoted by numbers $1'$ to $3'$) originate from the band gap of silicene in the three well regions with a magnitude of $2\Delta_{SO}$. For silicene superlattices with a larger number of barriers, more gap regions are formed, as shown in Fig. 3(a). Thus, the current, which is investigated later, is expected to decrease as the number of barriers increases. The relationship of the current-voltage characteristics is discussed later.

Similarly, the effect of the changing lateral width on the transmission spectrum can be understood by comparison of Fig. 3(a) ($a = b = 50$ nm) and Fig. 3(c) ($a = b = 10$ nm).
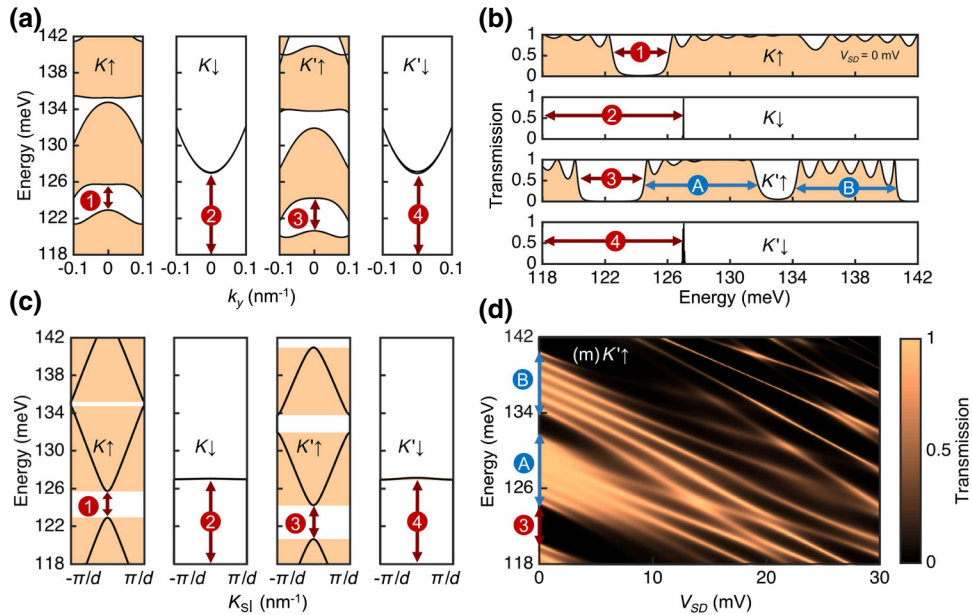

FIG. 2. Band structure and transmission spectra of the silicene superlattice with a ferromagnetic insulator. (a) Energy band structure of silicene superlattice as a function of wave vector k_y for four combinations of spin and valley flavors. Filled areas indicate the allowed bands. (b) Energy band structure of the silicene superlattice as a function of the Bloch-wave vector for normal incidence $k_y = 0$ nm^{-1}. (c) The unbiased transmission spectrum for eight-barrier silicene superlattices with lateral widths $a = b = 50$ nm and staggered sublattice potential $\Delta_Z = 40$ meV. (d) Transmission spectrum as a function of bias voltage V_{SD} for spin-up electrons in the K' valley. The potential barrier and exchange-splitting energy are $U = 175$ meV and $\Delta_{ex} = 36$ meV, respectively.
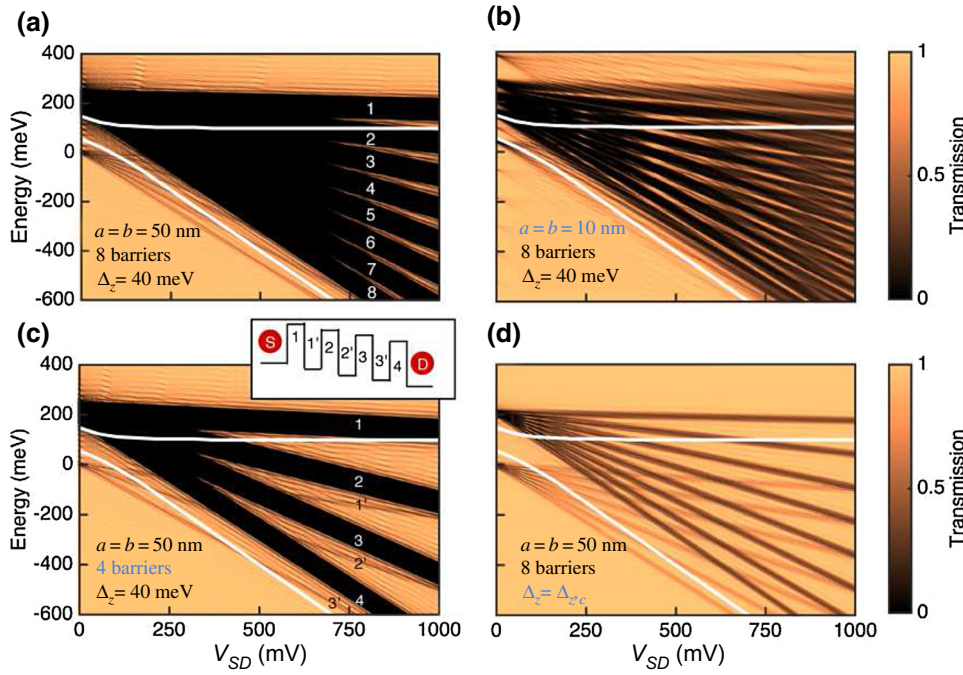
FIG. 3. Bias-dependent transmission spectra. (a) Bias-dependent transmission spectra for spin-up electrons in the K' valley with larger bias and energy range than that in Fig. 2(d). The lateral width, number of barriers, and staggered sublattice potential are $a = b = 50$ nm, $N = 8$, and $\Delta_Z = 40$ meV, respectively. The transmission spectra for (b) narrower width $a = b = 10$ nm, (c) lower number of barriers $N = 4$, and (d) smaller staggered sublattice potential $\Delta_{Z,C} = \Delta_{SO} = 3.9$ meV. The transport windows are denoted by the regions between two white lines.

For $a = b = 10$ nm, we find that the lateral width is too small to form an ideal gap (zero transmission). Therefore, the current in such silicene superlattices for such narrow lateral width is expected to be larger than that for wider lateral widths. Figure 3(d) shows the transmission spectrum of the silicene superlattices with a critical staggered sublattice potential $\Delta_Z = \Delta_{Z,C}$ in the barrier region, which is very small compared with the one in Fig. 3(a), leading to a thinner band gap. Thus, the current for the silicene superlattices with larger values of Δ_Z is expected to be smaller.

E. Spin- and valley-dependent NDR

Next we investigate the spin- ($s = \uparrow, \downarrow$) and valley-($\tau = K', K$) dependent current-voltage characteristics of the silicene superlattices, which can be obtained with the Landauer-Buttiker formula [36]:

$$
I_{\tau s} = \frac{2e}{h} \int_{-\infty}^{\infty} \{ T_{\tau s}(E, V_{SD}) \\
\times [f(E - \mu_S) - f(E - \mu_D)]\} dE, \quad (4)
$$

where $T_{\tau s}(E, V_{SD})$ is the bias-dependent transmission probability, $f(\varepsilon) = [\exp(\varepsilon/k_B T) + 1]^{-1}$ is the Fermi-Dirac distribution at temperature T, and μ_S (μ_D) is the chemical potential for the source (drain) electrode. The spin- and valley-resolved current can be defined as $I_s = I_{Ks + K's}$ and $I_\tau = I_{\tau \uparrow, \tau \downarrow}$, respectively.

Figure 4 shows the spin-resolved (upper panel) and valley-resolved (lower panel) current at room temperature as a function of the bias voltage. The parameters used in Figs. 4(a)–4(d) correspond to those used in Figs. 3(a)–3(d).

Two phenomena are observed: First, in Fig. 4(a), for both spin- and valley-resolved current, a relatively strong NDR effect at low bias voltage is observed, compared with that observed in Figs. 4(b)–4(d). This observation can be explained by the band-gap formation explored in Fig. 3: larger band-gap regions are formed in Fig. 3(a) than in Figs. 3(b)–3(d). Thus, stronger current suppression is expected, resulting in the strong NDR effect observed in Fig. 4(a). Second, the polarization of the spin-resolved current is stronger than that of the valley-resolved current. This result can be explained by the band structure, as shown in Fig. 2(b). Owing to exchange splitting induced by the ferromagnetic insulator, the band structures of spin-up and spin-down electrons are quite different, resulting in a large spin polarization, while the band structure of electrons in the K valley and the K' valley shows relatively small differences, leading to a small valley polarization. Unlike traditional semiconductor-based NDR devices, the incorporation of spin and valley degrees of freedom leads to richer phenomena in these NDR devices. Characteristics of this NDR device, such as the spin and valley physics and the behavior of the NDR effect can be better understood by our considering the band structure and transmission spectra of the superlattices.

F. Optimization of NDR devices

To optimize NDR devices that could be applied to logic-circuit designs, such as multistate inverter functions, the total current of the silicene superlattices, defined as $I = I_\uparrow + I_\downarrow = I_K + I_{K'}$, as a function of bias voltage V_{SD}, with variation of the number of barriers, lateral width, and
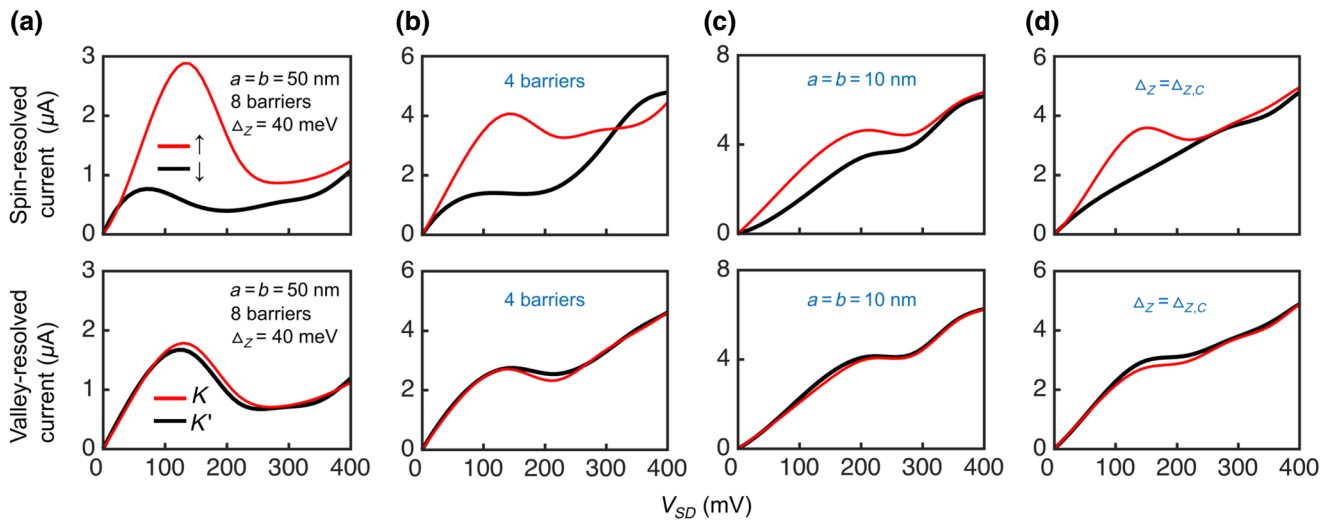
FIG. 4. Spin-resolved current I_S vs bias voltage V_{SD} [upper panels in (a)–(d)] and valley-resolved current I_V vs bias voltage V_{SD} [lower panels in (a)–(d)]. The parameters used in (a)–(d) are the same as those used in Figs. 3(a)–3(d), respectively.

staggered sublattice potential is further investigated. The results are shown in Fig. 5.

As shown in Fig. 3, increasing the three parameters leads to a well-formed band gap (approaching zero transmission) or a larger band-gap region. Therefore, the total current is expected to decrease as the three parameters increas from small values, as shown in Figs. 5(a)–5(c). When these parameters are too small to enable construction of the band-gap regions, the NDR effect is not obvious. As these parameters are increased, the NDR effect is stronger, and

can be quantitatively described by the PVCR. However, if we continue to increase these parameters, the PVCR might converge to a certain value or keep decreasing, depending on the different parameters: the PVCR will decrease for further increases in the number of barriers [Fig. 5(a)] and the magnitude of the staggered sublattice potential [Fig. 5(b)]. The PVCR eventually saturates for further increases of the lateral width [Fig. 5(c)]. This phenomena can be explained by the bias-dependent transmission spectra in Fig. 3: (i) increasing the number of barriers leads
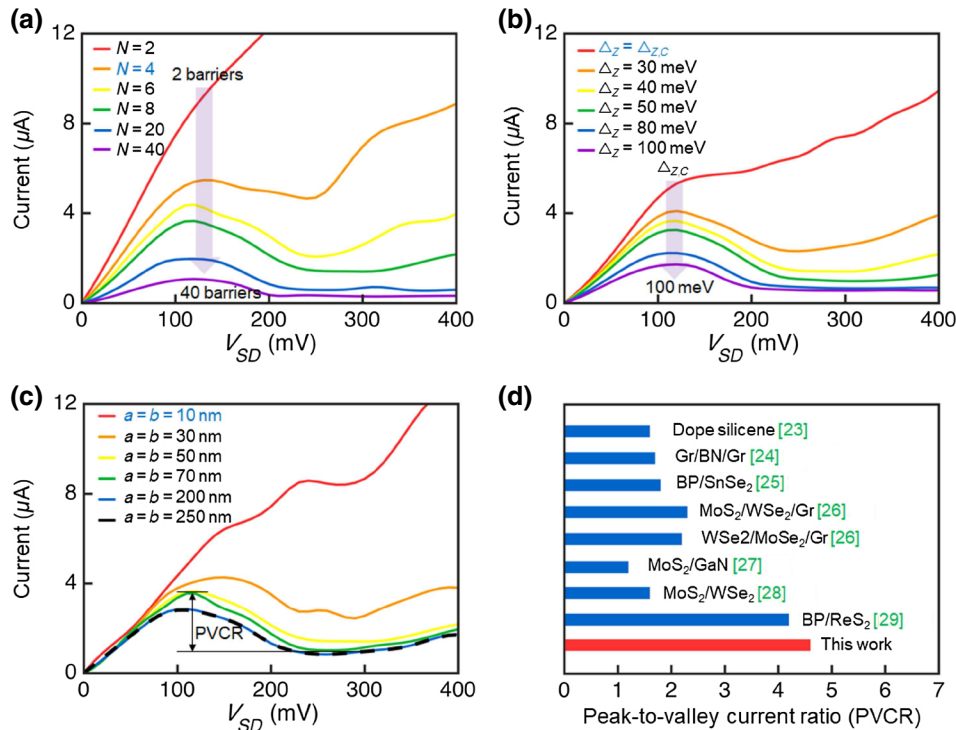

FIG. 5. Total current vs bias voltage V_{SD} at room temperature. Trend of the change of total current as a function of bias voltage V_{SD} for variation of (a) the number of barriers, (b) lateral widths, and (c) staggered sublattice potential. (d) Comparison of the PVCR in this work with other recently reported results at room temperature.

to more band gaps, and thus the current will continue to decrease; (ii) the increase of the staggered sublattice potential leads to a wider band gap, and thus the current will also keep decreasing; (iii) the increase of the lateral width makes the transmission in the band-gap region closer to zero. For a sufficiently thick lateral width, all the band gaps are well formed. Thus, the PVCR will converge to a certain value.

Moreover, the maximum value of the room-temperature PVCR obtained in this work is compared with other recently reported results based on 2D materials, as shown in Fig. 5(d). A room-temperature PVCR of up to 4.7 is the highest value in previously reported NDR devices made by layering of conducting channels. Notably, the operating voltage at this PVCR in this work is much smaller than the operating voltage reported with vertical structures [23–29] (see Fig. S1 in Supplemental Material [30]). However, our proposed structure features a lateral conducting path, suggesting that the silicene superlattice could be a good candidate for achieving NDR devices with low power consumption and high PVCR. Note that we use a ferromagnetic insulator to induce exchange-splitting energy in silicene superlattices. For those wanting to study the NDR effect in silicene without using ferromagnetic materials, we also examine a case of a nonmagnetic insulator, and these results are described in Figs. S2 and S3 in Supplemental Material [30].

IV. CONCLUSIONS

We demonstrate NDR devices based on silicene with a large room-temperature PVCR of up to 4.7 under a low operating bias, which is optimized by band-gap engineering of the silicene superlattices. Unlike traditional NDR devices, the spin and valley degrees of freedom of silicene are introduced into the proposed NDR devices, leading to a richer NDR effect. Moreover, we find that the tunable band gap in silicene and designable periods and lateral thicknesses of the superlattices have distinct effects on the band structure of the silicene superlattice and thus the NDR effect: (i) The band gap of silicene directly affects the size of the band gap in the silicene superlattice. We show that the NDR effect is not obvious for too large or too small a silicene band gap. Thus, an intermediate size for the silicene band gap, of approximately millielectronvolts, is needed to achieve a large PVCR. (ii) The period of the silicene superlattice determines the number of band gaps formed in graphene. Similarly, the NDR effect is not obvious for too many or too few periods. An appropriate number of periods in the range from 6 to 20 is also needed to optimize the NDR effect. (iii) The lateral thicknesses of the silicene superlattices determine how large the band gaps formed are. A maximum PVCR can be obtained for $a = b = 50$ nm. For large-enough lateral thicknesses

($a = b > 200$ nm), the band gaps are well formed. Therefore, the PVCR tends to become a constant for increasing thicknesses.

[1] K. S. Novoselov, A. K. Geim, S. V. Morozov, D. Jiang, Y. Zhang, S. V. Dubonos, I. V. Grigorieva, and A. A. Firsov, Electric field effect in atomically thin carbon films, Science **306**, 666 (2004).

[2] Y. Zhang, T. T. Tang, C. Girit, Z. Hao, Michael C. Martin, A. Zettl, Michael F. Crommie, Y. R. Shen, and Feng Wang, Direct observation of a widely tunable bandgap in bilayer graphene, Nature **459**, 820 (2009).

[3] C. H. Lui, Z. Li, K. F. Mak, E. Cappelluti, and T. F. Heinz, Observation of an electrically tunable band gap in trilayer graphene, Nat. Phys. **7**, 944 (2011).

[4] M. Ezawa, Valley-polarized Metals and Quantum Anomalous Hall Effect in Silicene, Phys. Rev. Lett. **109**, 055502 (2012).

[5] L. Tao, E. Cinquanta, D. Chiappe, C. Grazianetti, M. Fanciulli, M. Dubey, A. Molle, and D. Akinwande, Silicene field-effect transistors operating at room temperature, Nat. Nanotech. **10**, 227 (2015).

[6] L. A. Ponomarenko, R. V. Gorbachev, G. L. Yu, D. C. Elias, R. Jalil, A. A. Patel, A. Mishchenko, A. S. Mayorov, C. R. Woods, J. R. Wallbank, *et al.*, Cloning of dirac fermions in graphene superlattices, Nature **497**, 594 (2013).

[7] C. H. Park, L. Yang, Y. W. Son, M. L. Cohen, and S. G. Louie, Anisotropic behaviours of massless dirac fermions in graphene under periodic potentials, Nat. Phys. **4**, 213 (2008).

[8] Z. Sun, C. L. Pint, D. C. Marcano, C. Zhang, J. Yao, G. Ruan, Z. Yan, Y. Zhu, R. H. Hauge, and J. M. Tour, Towards hybrid superlattices in graphene, Nat. Commun. **2**, 559 (2011).

[9] M. Yankowitz, J. Xue, D. Cormode, J. D. Sanchez-Yamagishi, K. Watanabe, T. Taniguchi, P. Jarillo-Herrero, P. Jacquod, and B. J. LeRoy, Emergence of superlattice dirac points in graphene on hexagonal boron nitride, Nat. Phys. **8**, 382 (2012).

[10] G. L. Yu, R. V. Gorbachev, J. S. Tu, A. V. Kretinin, Y. Cao, R. Jalil, F. Withers, L. A. Ponomarenko, B. A. Piot, M. Potemski, *et al.*, Hierarchy of hofstadter states and replica quantum hall ferromagnetism in graphene superlattices, Nat. Phys. **10**, 525 (2014).

[11] R. V. Gorbachev, J. C. W Song, G. L. Yu, A. V. Kretinin, F. Withers, Y. Cao, A. Mishchenko, I. V. Grigorieva,

K. S. Novoselov, L. S. Levitov, *et al.*, Detecting topological currents in graphene superlattices, Science **346**, 448 (2014).

[12] M. Polini and F. H. L. Koppens, Graphene: Plasmons in moiré superlattices, Nat. Mater. **14**, 1187 (2015).

[13] M. Lee, J. R. Wallbank, P. Gallagher, K. Watanabe, T. Taniguchi, V. I. Fal'ko, and D. Goldhaber-Gordon, Ballistic miniband conduction in a graphene superlattice, Science **353**, 1526 (2016).

[14] T. P. Kaloni, M. Tahir, and U. Schwingenschlögl, Quasi free-standing silicene in a superlattice with hexagonal boron nitride, Sci. Rep. **3**, 3192 (2013).

[15] Zhi Ping Niu, Yong Mei Zhang, and Shihao Dong, Enhanced valley-resolved thermoelectric transport in a magnetic silicene superlattice, New J. Phys. **17**, 073026 (2015).

[16] T. T. Jia, M. M. Zheng, X. Y. Fan, Y. Su, S. J. Li, H. Y. Liu, G. Chen, and Y. Kawazoe, Band gap on/off switching of silicene superlattice, J. Phys. Chem. C **119**, 20747 (2015).

[17] Q. Zhang, K. S. Chan, and J. Li, Electrically controllable sudden reversals in spin and valley polarization in silicene, Sci. Rep. **6**, 33701 (2016).

[18] N. Missault, P. Vasilopoulos, F. M. Peeters, and B. Van Duppen, Spin-and valley-dependent miniband structure and transport in silicene superlattices, Phys. Rev. B **93**, 125425 (2016).

[19] J. Laskar, A. A. Ketterson, J. N. Baillargeon, T. Brock, Ilesanmi Adesida, K. Y. Cheng, and J. Kolodzey, Gate-controlled negative differential resistance in drain current characteristics of AlGaAs/InGaAs/GaAs pseudomorphic MODFETs, IEEE Electron. Dev. Lett. **10**, 528 (1989).

[20] J. P. A. van der Wagt, Tunneling-based sram, Proc. IEEE **87**, 571 (1999).

[21] E. Alekseev and D. Pavlidis, Large-signal microwave performance of GaN-based NDR diode oscillators, Solid State Electron. **44**, 941 (2000).

[22] L. Britnell, R. V. Gorbachev, A. K. Geim, L. A. Ponomarenko, A. Mishchenko, M. T. Greenaway, T. M. Fromhold, K. S. Novoselov, and Laurence Eaves, Resonant tunnelling and negative differential conductance in graphene transistors, Nat. Commun. **4**, 1794 (2013).

[23] Z. Ni, H. Zhong, X. Jiang, R. Quhe, G. Luo, Y. Wang, M. Ye, J. Yang, J. Shi, and J. Lu, Tunable band gap and doping type in silicene by surface adsorption: Towards tunneling transistors, Nanoscale **6**, 7609 (2014).

[24] A. Mishchenko, J. S. Tu, Y. Cao, R. V. Gorbachev, J. R. Wallbank, M. T. Greenaway, V. E. Morozov, S. V. Morozov, M. J. Zhu, S. L. Wong, *et al.*, Twist-controlled resonant tunnelling in graphene/boron nitride/graphene heterostructures, Nat. Nanotech. **9**, 808 (2014).

[25] R. Yan, S. Fathipour, Y. Han, B. Song, S. Xiao, M. Li, N. Ma, V. Protasenko, D. A. Muller, D. Jena, *et al.*, Esaki diodes in van der waals heterojunctions with broken-gap energy band alignment, Nano Lett. **15**, 5791 (2015).

[26] Y. C. Lin, R. K. Ghosh, R. Addou, N. Lu, S. M. Eichfeld, H. Zhu, M. Y. Li, X. Peng, M. J. Kim, L. J. Li, *et al.*, Atomically thin resonant tunnel diodes built from synthetic van der waals heterostructures, Nat. Commun. **6**, 7311 (2015).

[27] S. Krishnamoorthy, E. W. Lee II, C. H. Lee, Y. Zhang, W. D. McCulloch, J. M. Johnson, J. Hwang, Y. Wu, and S. Rajan, High current density 2D/3D MoS$_2$/GaN Esaki tunnel diodes, Appl. Phys. Lett. **109**, 183505 (2016).

[28] A. Nourbakhsh, A. Zubair, M. S. Dresselhaus, and T. Palacios, Transport properties of a MoS$_2$/WSe$_2$ heterojunction transistor and its potential for application, Nano Lett. **16**, 1359 (2016).

[29] J. Shim, S. Oh, D. H. Kang, S. H. Jo, M. H. Ali, W. Y. Choi, K. Heo, J. Jeon, S. Lee, M. Kim, *et al.*, Phosphorene/rhenium disulfide heterojunction-based negative differential resistance device for multi-valued logic, Nat. Commun. **7**, 13413 (2016).

[30] See Supplemental Material at http://link.aps.org/supplemental/10.1103/PhysRevApplied.10.044047 for additional figures.

[31] H. Haugen, D. Huertas-Hernando, and A. Brataas, Spin transport in proximity-induced ferromagnetic graphene, Phys. Rev. B **77**, 115406 (2008).

[32] A. G. Swartz, P. M. Odenthal, Y. Hao, R. S. Ruoff, and R. K. Kawakami, Integration of the ferromagnetic insulator EuO onto graphene, ACS Nano **6**, 10063 (2012).

[33] A. Hallal, F. Ibrahim, H. Yang, S. Roche, and M. Chshiev, Tailoring magnetic insulator proximity effects in graphene: first-principles calculations, 2D Mater. **4**, 025074 (2017).

[34] C. Núñez, P. A. Orellana, L. Rosales, R. A. Römer, and F. Domínguez-Adame, Spin-polarized electric current in silicene nanoribbons induced by atomic adsorption, Phys. Rev. B **96**, 045403 (2017).

[35] M. I. Katsnelson, K. S. Novoselov, and A. K. Geim, Chiral tunnelling and the Klein paradox in graphene, Nat. Phys. **2**, 620 (2006).

[36] S. Datta, *Electronic Transport in Mesoscopic Systems* (Cambridge University Press, New York, 1997).

[37] M. Spencer and T. Morishita, *Silicene: Structure, Properties and Applications* (Springer, Switzerland, 2016), Vol. 235.

[38] G. B. Liu, D. Xiao, Y. Yao, X. Xu, and W. Yao, Electronic structures and theoretical modelling of two-dimensional group-VIB transition metal dichalcogenides, Chem. Soc. Rev. **44**, 2643 (2015).